Dense-packed arrays on surfaces of constant negative curvature

Michael Rubinstein* and David R. Nelson
Department of Physics, Harvard University, Cambridge, Massachusetts 02138
(Received 8 August 1983)

Dense-packed assemblies of hard spheres are standard models of disorder in metallic glasses. Such packings are difficult to obtain with identical disks on flat two-dimensional surfaces because triangular packing units are easily incorporated into a hexagonal close-packed lattice. By packing disks on a two-dimensional manifold of constant negative curvature, however, one can study packing problems quite similar to those found in three-dimensional flat space.

I. INTRODUCTION

Structure in dense, supercooled liquids and in metallic glasses is closely related to the difficulty in filling space with tetrahedra of identical particles.[1–4] Frustration becomes evident in three-dimensional (3D) packing problems when 20 tetrahedra combine to form an icosahedron. As shown in Fig. 1(a), gaps appear between 12 symmetrically disposed surface particles. The atoms at the surface cannot simultaneously sit at the minima of the pair potential of the central atom and of their neighbors on the surface. Although simple pair potentials lead to a strong energetic preference locally for icosahedra,[5,6] any particle packing with local icosahedral order must be riddled with defects. The nature of these defects is suggested by Coxeter's observation that icosahedra of identical particles can be used to tile the surface of a four-dimensional sphere without frustration.[7–9] As pointed out by Kléman and Sadoc,[10] defects such as disclinations are necessary to map the four-sphere into flat space. The relevant defects have recently been characterized more precisely using homotopy theory[11] and the icosahedral order parameter defined in Ref. 6.[12] The Frank-Kasper phases of complex transition-metal alloys[13] are an interesting example of ordered arrays of frustration-induced disclination lines in an otherwise icosahedral medium. Structure in metallic glasses can be modeled by a disordered array of such lines.[12]

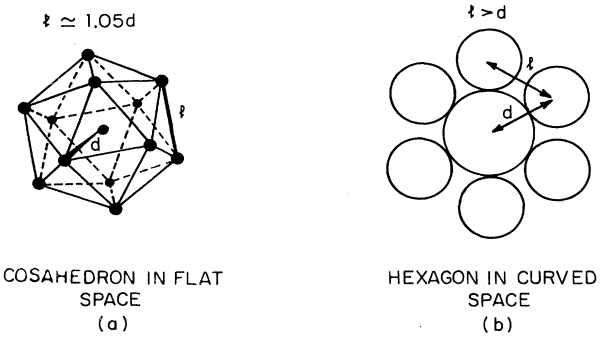

FIG. 1. Comparison of the icosahedron in flat space, and a hexagon projected out of a space of constant negative curvature. In both cases, the distance l between the centers of the particles on the surface is larger than the distance d to the center.

In this paper, we study similar dense random packing problems in two dimensions. It is, of course, easier to construct and discuss analytically particles packed on a surface instead of in $d=3$ dimensions. There are, in addition, elegant techniques based on the Dirichlet construction for visualizing defects[14,15] when such packings are viewed from the third dimension. The two-dimensional (2D) figure most analogous to the icosahedron is a hexagon composed of six identical triangular packing units. There is, unfortunately, no frustration, since the hexagon can be periodically extended to tile the plane. Frustration can be introduced into planar arrays of particles by allowing for two different particle sizes.[16–19] The resulting disorder is fundamentally different, however, than in 3D flat space. There is, in particular, no analog of the asymmetry between plus and minus disclinations expected in three dimensions.[12]

Frustration like that in 3D flat space does appear when identical disks are packed on a surface $H2$ of constant negative curvature.[12,20] As shown in Fig. 1(b), cracks open up between the disks at the surface of a hexagon. The curvature of this surface is a tunable parameter which can be used to vary the frustration. When the curvature is nonzero, one has the same difficulty in filling space with equilateral triangles as for perfect tetrahedra in 3D flat space. We report here on computer-generated arrays of hard disks placed on these surfaces via a simple deterministic packing algorithm. The procedure is a 2D version[18] of one used by Bennett[3] to generate packings of hard spheres. Using this method, one can easily generate arrays with large numbers of particles. Although the only "randomness" is associated with round-off errors in the computer, 3D Bennett models, when relaxed in a soft potential, have properties remarkably similar to real metallic glasses.[21]

Although the hyperbolic space $H2$ cannot be embedded in three dimensions, the resulting particle packings can be visualized in projection. A related projection of particles on the *positively* curved surface of a sphere is shown in Fig. 2.[22] Particles labeled by spherical polar coordinates were packed using Bennett's procedure, starting at the north pole of the sphere. The crude projection shown in Fig. 2 was obtained by identifying the spherical polar coordinates with ordinary plane polar coordinates. More

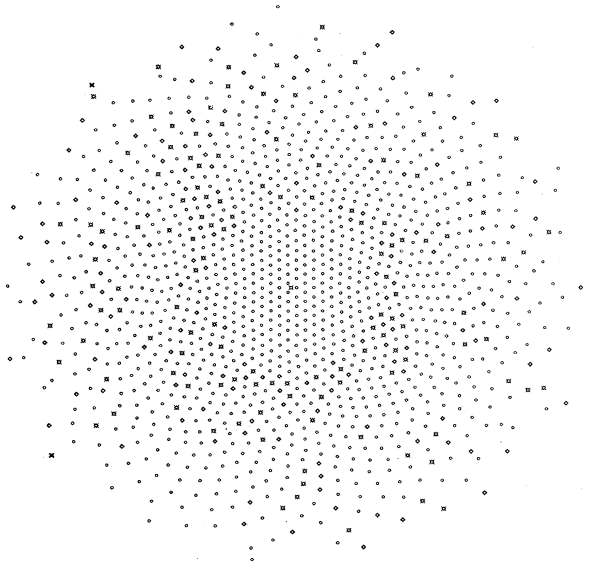

FIG. 2. Array of 1314 identical disks packed by the Bennett algorithm on the surface of the sphere with radius ten times the disk diameter. The projection used is $r'=r$, $\phi'=\phi$, where (r,ϕ) are spherical polar coordinates and (r',ϕ') are plane polar coordinates. The north pole marked by the square is chosen as the center of the planar coordinate system as well as the center of the Bennett cluster. Anomalous 5- and 7-coordinated points are devoted by diamonds and asterisks, respectively.

sophisticated projection schemes will be used to display hyperbolic particle packings in Sec. II.

Figure 2 also illustrates the "5-7 construction,"[14,15] which will be used to study defects. A curved-space generalization of the Dirichlet construction is used to generate a "Wigner-Seitz" cell around every atom, separating it from its near neighbors. The boundaries of the cell are geodesics. The number of sides of the Dirichlet polygon gives the coordination number of the particle. In Fig. 2, anomalous 5- and 7-coordinate particles are highlighted by diamonds and asterisks, respectively. Most particles have coordinate number 6. In flat space, the 5's and 7's can be viewed as microscopically defined disclinations with "charges" $+1$ and -1. Dislocations appear as 5-7 pairs.[15] Note that the packing in Fig. 2 appears to be a hexagonal close-packed lattice until curvature-induced defects start to appear at sufficiently large distances from the north pole. We have observed the same effect in a hyperbolic counterpart of Fig. 2. Analogous difficulties are encounted when one tries to make large clusters with an icosahedral symmetry in 3D flat space.[23]

The average coordination number in 2D flat space must be exactly 6,[14] which makes particle configurations in this case topologically rather uninteresting. Nontrivial questions arise, however, for incommensurate, nonzero curvatures. The hyperbolic spaces studied here are characterized by a metric, which in polar coordinates (r,ϕ) reads[9]

$$d^2s=d^2r+[\sinh(\kappa r)/\kappa]^2d^2\phi\ . \tag{1.1}$$

The Gaussian curvature of the space K is related to the parameter κ by $K=-\kappa^2$. The quantity κ^{-1} is an intrinsic frustration length scale, which tends to infinity as space becomes flat. [For a sphere with positive Gaussian curvature κ^2, $\sinh(\kappa r)$is replaced by a $\sin(\kappa r)$ where κ^{-1} is the radius of the sphere.] It is a simple application of the Gauss-Bonnett theorem to show that the average coordination $\bar{Z}$ in a space of constant Gaussian curvature K is[20,24]

$$\bar{Z}=6-3Ks/\pi\ , \tag{1.2}$$

where s is the surface area per particle. Because the surface area per particle enters Eq. (1.2), the average coordination number is not automatically determined by the properties of the space when K is nonzero. The disordered, hyperbolic Bennett packings we have studied are characterized by $\bar{Z}$'s which are quite close to an ideal value (corresponding to an ideal packing fraction) predicted by a simple "statistical-honeycomb" model, similar to a statistical honeycomb studied by Coxeter in three dimensions.[7,9]

Our results are described in detail in Sec. II. Overall, we find that disordered tessellations of $H2$ are remarkably similar to dense random packing in three dimensions. We find, in analogy with three dimensions, a split-second peak in the radial distribution function. There is an asymmetry in the distribution of point disclination defects, similar to that predicted for disclination lines in three dimensions.[12] Hexagonal orientational order is broken up by these defects in a way remininscent of the decay of icosahedral order found by Steinhardt *et al.*[6] We also investigate features which have no simple analog in three dimensions, such as transitions to commensurate sevenfold and eightfold lattices when the curvature becomes sufficiently negative.

Improvements in the procedures used here are certainly possible. It is well known that Bennett's packing procedure leads to anomalous density correlations in the radial direction.[25] Such unwanted correlations could be eliminated by relaxing the particles in a softer potential. Studies of relaxation and kinetics via Monte Carlo or molecular-dynamics techniques would of course be especially interesting. Real metallic glasses in three dimensions require particles with two different sizes. As discussed in Ref. 12, the smaller phosphorus atoms in an alloy like CoP are nodes for disclination lines with the "wrong" sign—the charge of these lines is opposite to that needed to relax the topological frustration. It is possible to mimic this effect in $H2$ by introducing a dilute concentration of small particles which can only accommodate five near neighbors. Since sevenfold disclinations are favored over fivefold charges in $H2$, here too one would be seeding the material with disclinations of the wrong sign.

II. RESULTS

A. Basic concepts

The properties of the hyperbolic space $H2$ are determined by the metric (1.1), expressed in terms of polar coordinates r and ϕ.[26] Polar coordinates are essential to discuss the global properties of $H2$, because it is impossi-

ble to introduce a singularity-free Cartesian coordinate system. In order to pack particles on the computer, we integrate Eq. (1.1) to obtain the geodesic distance l_{ab} between two points with polar coordinates (r_a,ϕ_a) and (r_b,ϕ_b):

$$\cosh(\kappa l_{ab})=\cosh(\kappa r_a)\cosh(\kappa r_b) -\sinh(\kappa r_a)\sinh(\kappa r_b)\cos(\phi_a-\phi_b) . \quad (2.1)$$

The integration is carried out explicitly in Appendix A. Hard disks with diameter d were deposited sequentially starting with a seed configuration of three particles forming an equilateral triangle centered at the origin. Successive disks were brought into contact with the growing seed cluster so that (1) each new disk just touched two previously deposited disks without ovelapping any part of the seed; and (2) the distance to the origin [as determined by Eq. (2.1)] was as small as possible. Starting with a tetrahedral seed cluster, Bennett has used a similar algorithm to generate disordered particle arrays in 3D flat space.[3]

Significant differences in particle packings are expected as a function of the dimensionless parameter κd.[20] Consider n particles symmetrically arranged about a central disk as in Fig. 1(b). For each value of n, there is a special "commensurate" curvature such that these $n+1$ particles form a regular polygon with no gaps between the hard disks at the surface. Each regular polygon is then composed of n identical equilateral triangles with angles $2\pi/n$. (In hyperbolic space, of course, the sum of the angles of a triangle is no longer equal to π.[26]) It is easy to use (2.1) to show that the commensurate curvatures are given by[12,20]

$$\kappa_n d=2\cosh^{-1}\left[\frac{1}{2\sin(\pi/n)}\right] . \quad (2.2)$$

When κd equals one of the special values given by Eq. (2.2), one might expect the Bennett packing algorithm to lead to a regular "crystalline" lattice, analogous to the hexagonal lattice obtained for the flat-space case $n=6$. Because there is no global Cartesian coordinate system for $\kappa d\neq 0$, flat-space ideas about what constitutes a "lattice" must be modified.[27] Our definition of a regular n-fold lattice requires that all particles have Dirichlet coordination number n, and that there are δ-function peaks at discrete intervals in the radial distribution $g(r)$ (see Sec. II D). The regular eightfold tessellation we find when κd equals

$$\kappa_8 d\approx 1.528\,57 \quad (2.3)$$

is like a flat-space Bravais lattice with inversion symmetry, while the heptagonal lattice corresponding to

$$\kappa_7 d\approx 1.090\,55 \quad (2.4)$$

is like a Bravais lattice with a basis—similar to a honeycomb lattice in flat space.

The surface area per particle for the commensurate tessellations is determined by the topological constraint (1.2), which we write as

$$\bar{Z}(\kappa,s)=6+3\kappa^2 s/\pi . \quad (2.5)$$

Since $\bar{Z}=n$ for the n-fold lattices defined above, the surface area per particle s_n for the ideal structure in a commensurate curvature κ_n is

$$s_n=\pi(n-6)/3\kappa_n^2 . \quad (2.6)$$

Since the area of a disk of diameter d in hyperbolic space is

$$s_{\text{disk}}=\int_0^{2\pi}d\phi\int_0^{d/2}\frac{\sinh(\kappa r)}{\kappa}dr =4\pi\sinh^2(\kappa d/4)/\kappa^2 , \quad (2.7)$$

the packing fraction f_n is

$$f_n\equiv s_{\text{disk}}/s_n=\frac{3/\sin(\pi/n)-6}{n-6} , \quad (2.8)$$

where we have used the expression for the commensurate curvature (2.2). The packing fraction (2.8) reduces to the familiar result $f_6=\pi/2\sqrt{3}\approx 0.907$ for a flat-space hexagonal lattice and gives $f_7\approx 0.914$, $f_8\approx 0.920$, and $f_9\approx 0.924$. The packing fraction is a monotonically increasing function of coordination number, because the relative area occupied by the cracks in an n-fold lattice of hard disks decreases with n.

In this paper, we shall focus primarily on incommensurate curvatures $0=\kappa_6<\kappa<\kappa_7$. An ideal packing fraction $f_{\text{ideal}}(\kappa d)$ can be defined for *general* curvatures by analytically continuing Eqs. (2.2) and (2.8) off the integers. With every value of κd, we associate a lattice of identical Dirichlet polygons, which must in general have nonintegral numbers of sides. Solving Eq. (2.2) for $n=\bar{Z}_{\text{ideal}}$, we see that the coordination number of this "statistical-honeycomb" lattice is

$$\bar{Z}_{\text{ideal}}(\kappa d)=\pi\left[\sin^{-1}\left[\frac{1}{2\cosh(\kappa d/2)}\right]\right]^{-1} . \quad (2.9)$$

Replacing n by $\bar{Z}_{\text{ideal}}$ in Eq. (2.8) gives us an "ideal" packing fraction for every value of κd. It seems plausible that $f_{\text{ideal}}(\kappa d)$ represents a preferred packing fraction in an unbounded space of constant negative curvature. This ideal packing fraction varies monotonically from $\pi/2\sqrt{3}$ when $\kappa d=0$, to $3/\pi$ as κd tends toward infinity. In general, one expects the packing fraction in highly disordered particle configurations to be smaller than the ideal value. As we shall see, particles packed via Bennett's procedure have packing fractions quite close to the ideal value, even when the curvature is incommensurate.

Remarkably similar issues arise when particles are packed in 3D flat space. Just as one can "triangulate" a 2D particle configuration with near-neighbor bonds via the Dirichlet construction, one can construct a tetrahedral array of bonds joining near neighbors via the Voronoi construction in three dimensions. The particle coordination number on a 2D surface is also the number of triangles surrounding that particle. As stressed in Ref. 12, the analogous concept in three dimensions is the number of tetrahedra q surrounding a *bond*. A lattice of perfect tetrahedra is impossible, since the curvature of 3D flat space is incommensurate. The average number of tetrahedra surrounding a bond $\bar{q}$ will in general increase with the

degree of disorder. A simple physical argument[12] suggests, however, that tetrahedral particle packings corresponding to an "ideal glass" will have

$$\bar{q}=\bar{q}_{\text{ideal}}=2\pi/\cos^{-1}(\tfrac{1}{3})$$
$$=5.104\,299\ . \tag{2.10}$$

The value of $\bar{q}$ for the Frank-Kasper phases differs from (2.10) by a few parts in ten thousand. The result in Eq. (2.10) was first obtained by Coxeter for a fictitious statistical-honeycomb particle tessellation, such that every bond is surrounded by the same fractional number of perfect tetrahedra.[7,9] Equation (2.9) applies to an analogous 2D statistical honeycomb. In this sense, $\bar{q}_{\text{ideal}}$ in 3D flat space is the analog of the quantity $\bar{Z}_{\text{ideal}}$ defined for a range of incommensurate curvatures by Eq. (2.9).

The concept of a "packing fraction" makes more physical sense for hard disks than for particles interacting via soft pair potentials. As stressed, for example, in Ref. 23, frogs eggs and caviar are a better model of, say, rare gas atoms packed at low temperatures than hard spheres. It also seems awkward to describe simple metals, which are well approximated by *point* ions immersed in an essentially incompressible sea of conduction electrons, by packing fractions. For this reason, it is probably best to summarize our results in terms of purely topological concepts, like the average coordination number. One can always use Eqs. (2.5) and (2.8) to convert results for $\bar{Z}$ into packing fractions for the special case of hard disks.

B. Particle packings

As discussed in the Introduction, an appealing feature of 2D glassy particle configurations is that they can be viewed from the third dimension. When the 5-7 construction is used to highlight defects, one obtains a graphic representation of the disorder which is difficult to achieve in three dimensions. Particle packings in hyperbolic space can be viewed by projecting them onto a plane. Although projections which preserve distances are impossible, one can find mappings of $H2$ into flat space which preserve angles or transform geodesics into straight lines.[27] Given a point with hyperbolic polar coordinates (r,ϕ), a projection procedure is defined by *plane* polar coordinates (r',ϕ'), where r' and ϕ' are functions of r and ϕ. Figure 3(a) shows a conformal projection of 1000 particles packed via Bennett's algorithm with $\kappa d=0.5$. Anomalous coordination numbers are highlighted using the procedure discussed in the Introduction. This angle-preserving projection is defined by[27]

$$r'=R_0\tanh(\kappa r/2),\quad \phi'=\phi\ , \tag{2.11}$$

where R_0 is the radius of the disk into which all of $H2$ is mapped. Unfortunately, most of the particles are squeezed into a narrow strip near the rim of the disk. This distortion of distance is even more severe for the geodesic projection, which maps geodesics into straight lines via[27]

$$r'=R_0\tanh(\kappa r),\quad \phi'=\phi\ . \tag{2.12}$$

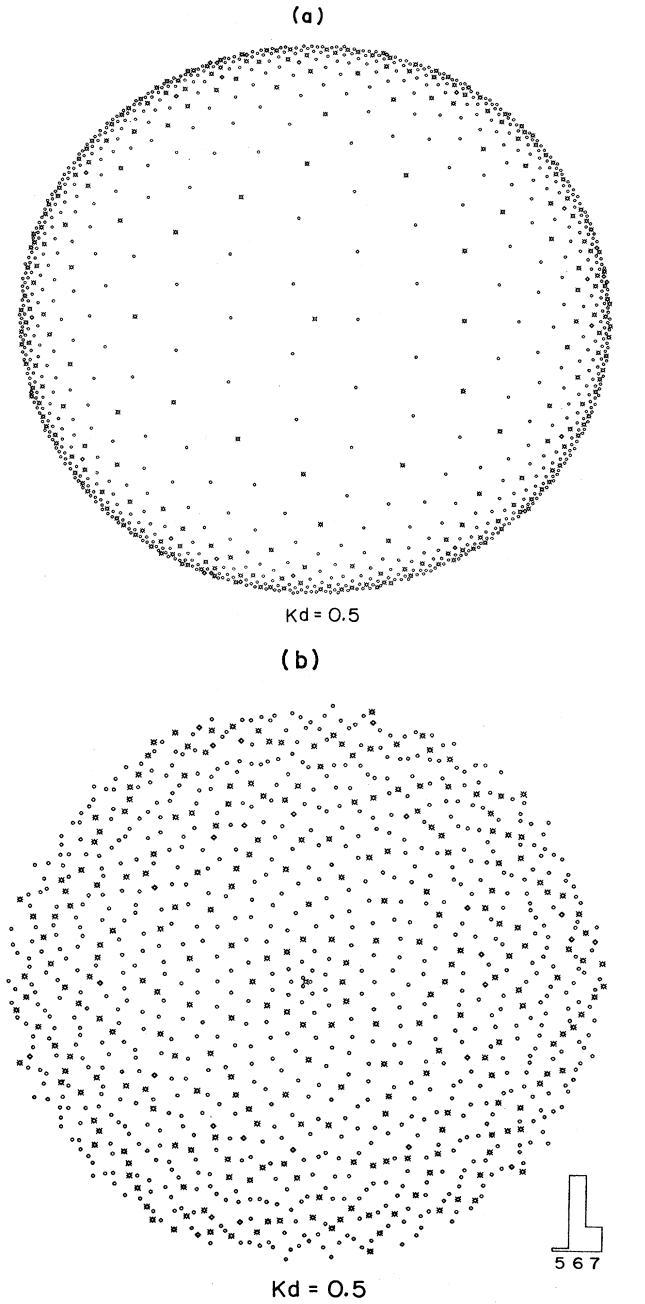

FIG. 3. (a) Conformal map of 1000 disks packed by the Bennett algorithm on a surface of uniform negative curvature with $\kappa d=0.5$. (b) The same configuration mapped by $r'=r^{1+\kappa d}$, $\phi'=\phi$. Histogram indicates the relative numbers of fivefold–sevenfold coordinated points.

We have found it preferable to use a projection scheme which does not distort distances so severely, namely

$$r'=d(r/d)^{1+\kappa d},\quad \phi'=\phi\ . \tag{2.13}$$

As illustrated in Fig. 3(b), for the same packing as in Fig. 3(a), this *ad hoc* algorithm produces an approximately homogeneous distribution of 1000 particles in the plane,

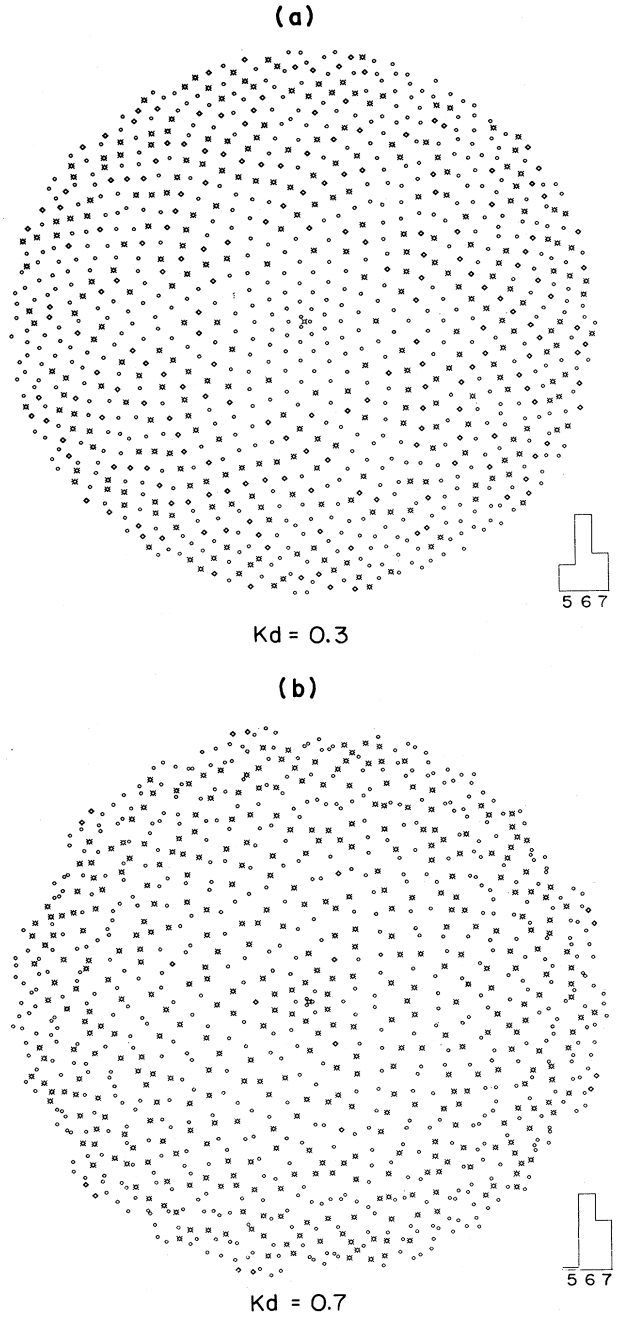

FIG. 4. Array of 1000 disks packed on the surface of constant negative curvature, plotted by the same map as Fig. 3(b) for (a) $\kappa d = 0.3$ and (b) $\kappa d = 0.8$.

and gives a clear impression of the defect topology. It also reduces to flat-space polar coordinates in the limit $\kappa d \to 0$.

Packings of identical disks projected using Eq. (2.13) are shown in Figs. 4(a) and 4(b) for $\kappa d = 0.3$ and $\kappa d = 0.7$, respectively. The 1000 particles shown in these figures were extracted from the centers of approximately 2000 particle arrays to eliminate edge effects. When comparing these particle packings with Fig. 3(b), it is helpful to also examine the coordination-number histograms shown in the insets. Although six-coordinated particles dominate in all three cases, the bias toward seven-coordinated particles, as opposed to five-coordinated particles predicted by Eq. (2.5) is quite evident. A similar-asymmetry appears in the distribution of tetrahedra per bond in 3D dense random packings.[12] One candidate for the ground state is a regular arrangement of sevenfold disclinations embedded in an otherwise six-coordinated medium. Evidently, these highly ordered ground states are not accessible via Bennett's packing procedure. The degree of disorder evident in the figures is related to the number of unpaired fivefold disclinations. We would expect qualitatively similar particle configurations for finite-temperature systems cooled on a hyperbolic manifold at rates which are fast compared to the time necessary to equilibrate disclinations. The configuration for $\kappa d = 0.3$ is clearly more ordered near the initial seed triangle. The influence of the seed is less evident for $\kappa d = 0.5$ and $\kappa d = 0.7$. All three particle configurations display a weak, threefold asymmetry aligned with the orientation of the initial seed triangle. The asymmetry decreases with increasing distance from the center. More homogeneous particle configura-

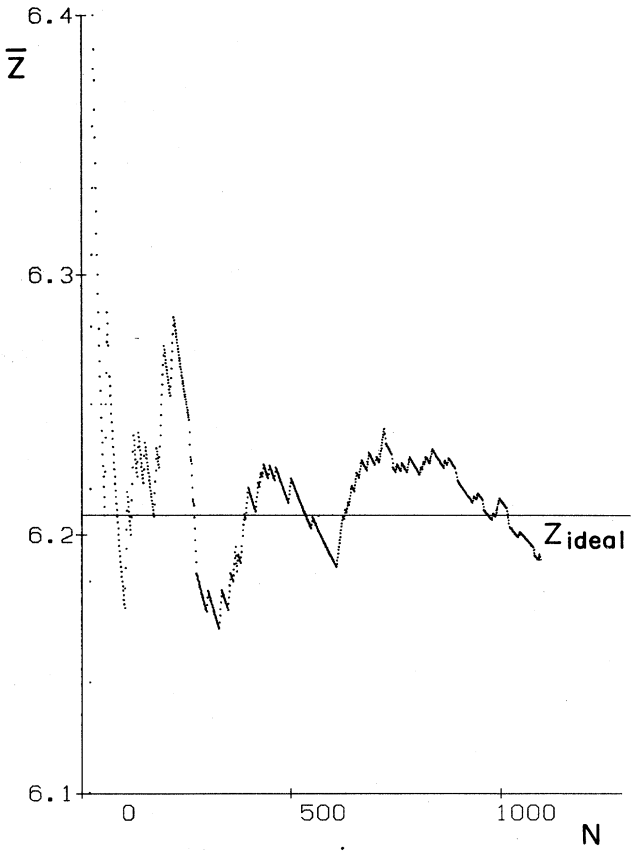

FIG. 5. Average coordination number $\bar{Z}$ as a function of the number of N disks packed sequentially on the surface of constant negative curvature with $\kappa d = 0.5$. Straight line corresponds to $\bar{Z}_{ideal}$.

TABLE I. Numerical data for particles packed at a variety of incommensurate curvatures. This information pertains to a 1000-disk central portion of computer-generated 2000-particle arrays.

κd	N_5	N_6	N_7	$\bar{Z}$	$\bar{Z}_{\text{ideal}}$	f	f_{ideal}	d_1	d_2	ξ_6
0.3	189	544	267	6.08	6.075	0.908	0.9075	1.74	2.00	3.0
0.4	102	648	250	6.15	6.133	0.908	0.9080	1.74	2.00	2.3
0.5	27	733	240	6.21	6.207	0.909	0.9087	1.72	2.00	2.1
0.6	39	619	342	6.30	6.299	0.909	0.9094	1.72	2.00	1.9
0.7	18	595	387	6.37	6.408	0.910	0.9102	1.70	2.00	2.0
0.8	0	466	534	6.53	6.534	0.911	0.9112	1.70	2.00	2.0

tions would presumably result from relaxing these Bennett packings in a softer pair potential.[25]

Figure 5 shows the average coordination number $\bar{Z}$ for the first N particles in the cluster. These results are consistent with an oscillatory approach to a value close to that predicted by the statistical-honeycomb model, $\bar{Z}_{\text{ideal}}(\kappa d=0.5)\approx 6.207$. The Frank-Kasper phases in 3D flat space exhibit very similar behavior when $\bar{q}$ is plotted as a function of the size of the unit cell.[12] The surface area per particle, and hence the packing fraction, can be extracted from Eq. (2.5). A summary of our numerical results for six different values of κd is contained in Table I.

C. Correlation functions

The radial distribution function $g(r)$ for $\kappa d=0.5$ is shown in Fig. 6. The definition of this function is a generalization of the flat-space one[2]; we define $g(r)$ to be the average number of particles with geodesic distances between r and $r+dr$ from a given one divided by the area of the corresponding annulus: $2\pi[\sinh(\kappa r)/\kappa]dr$. The second peak of this distribution function appears to be split into two subpeaks in a way reminiscent of 3D dense random packing[1–3,28] and of experimentally[29] determined radial distribution functions for metallic glasses. The position of the first subpeak can be calculated as the length of the longer diagonal d_1 of a rhombus in $H2$ with sides d and the shorter diagonal equal to d:

$$d_1=\frac{1}{\kappa}\cosh^{-1}\left[\frac{4\cosh^2(\kappa d)}{\cosh(\kappa d)+1}-1\right]. \tag{2.14}$$

For $\kappa d=0.5$ one finds $d_1\approx 1.715d$ in good agreement with the position of the first subpeak $1.72d\pm 0.01d$. The second main subpeak is at $d_2\simeq 2d$ implying the existence of three-membered collinearity similar to those noted for 3D random-packed models.[1–3,28]

At large separations the radial distribution function should approach the average number density s^{-1}, which can be determined from the average coordinate number via Eq. (2.5). Using the value of $\bar{Z}$ in Table I, we find $s^{-1}=1.14d^{-2}$ for $\kappa d=0.5$. The asymptotic behavior of Fig. 6 is consistent with this value.

Another quantity of interest is the orientational order parameter $\psi_6(\vec{r})$. In 2D flat space, this quantity is given by[17]

$$\psi_6(\vec{r})=e^{6i\theta(\vec{r})}, \tag{2.15}$$

where $\theta(\vec{r})$ is the angle a bond (joining two near-neighbor atoms and centered at $\vec{r}$) makes with respect to some reference axis. It is difficult to define an average like $\langle\psi_6(\vec{r})\rangle$ precisely in curved space, because one cannot unambiguously specify a reference axis for $\theta(\vec{r})$ common

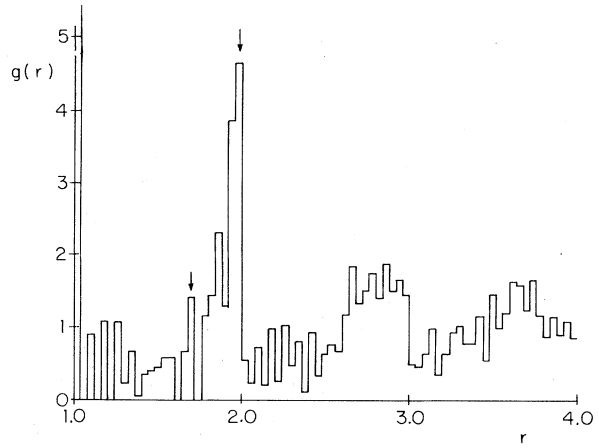

FIG. 6. Radial distribution function for the cluster plotted in Fig. 3.

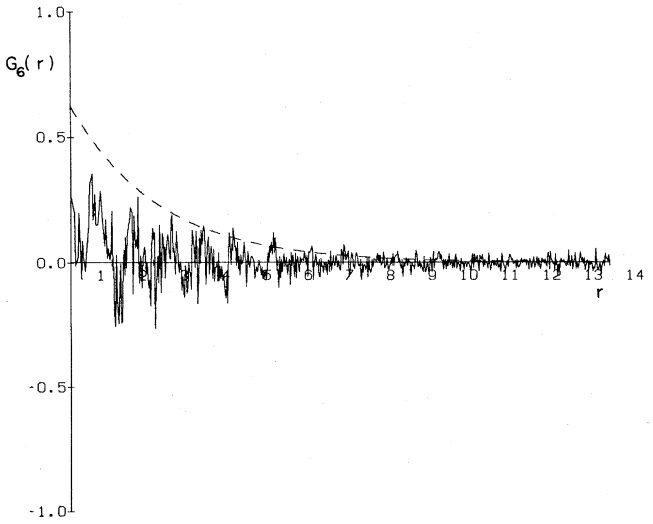

FIG. 7. Orientational correlation function for the cluster plotted on Fig. 3.

to all of $H2$.[12] It is possible, however, to define a *path-dependent* correlation function

$$G_{\Gamma}^{(6)}(\vec{r}) \equiv \langle \psi_6^*(\vec{0})\psi_6(\vec{r})\rangle_{\Gamma} , \tag{2.16}$$

where the angles $\theta(\vec{r})$ ane $\theta(\vec{0})$ entering Eq. (2.16) are to be compared after the bond at $\vec{r}$ is parallel transported to the origin along a path Γ. It is a straightforward exercise in differential geometry to show that the correlations along two different paths Γ and Γ' are related,

$$G_{\Gamma'}^{(6)}(\vec{r}) = G_{\Gamma}^{(6)}(\vec{r}) e^{6i\kappa^2 S_{\Gamma\Gamma'}} , \tag{2.17}$$

where $S_{\Gamma\Gamma'}$ is the surface area contained in the closed contour traced by first following the path Γ from $\vec{r}$ to $\vec{0}$, and then taking the path Γ' from $\vec{0}$ back to $\vec{r}$. This area is counted with a positive sign for counterclockwise circuits, and with a negative sign for clockwise ones. Thus, correlation functions defined by different paths are related by a simple phase factor. Path-dependent spin-correlation functions behave in a similar way for uniformly frustrated XY spin models in 2D flat space.[30]

In practice, it is most straightforward to compute $G_{\Gamma}^{(6)}(\vec{r})$ choosing Γ to be the *geodesic* path Γ_0 joining the

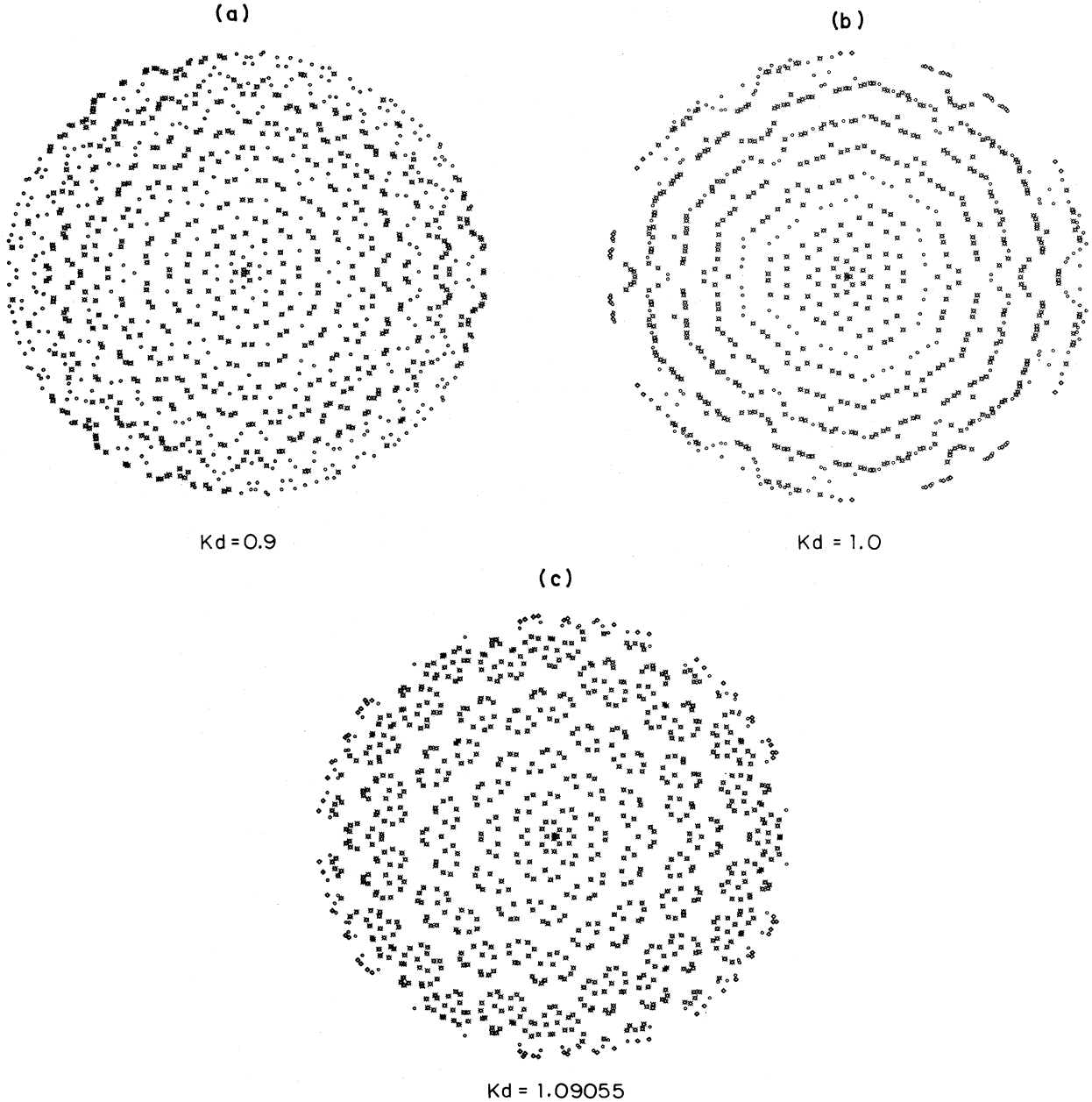

FIG. 8. Commensurate-incommensurate transition plotted by the same map as Fig. 3(b). Arrays of 1000 disks packed on the surface of constant negative curvature with (a) $\kappa d = 0.9$, (b) $\kappa d = 1.0$, and (c) $\kappa d = 1.090\,55$. The coordination number of a few outside disks is affected by the boundary.

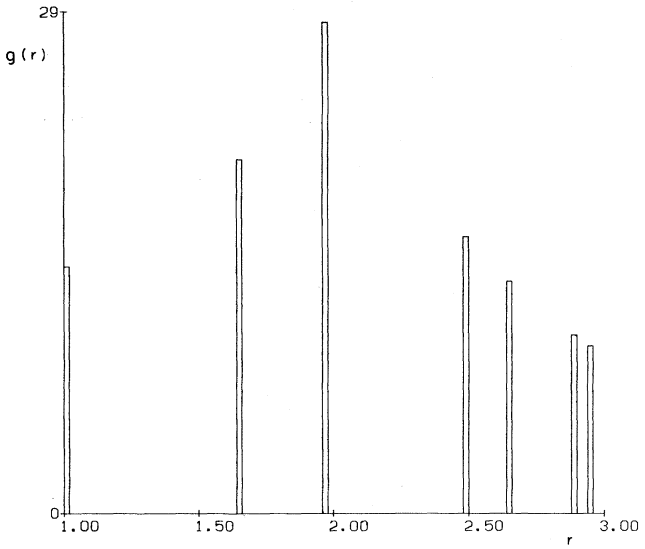

FIG. 9. Radial distribution function $g(r)$ for the array plotted on Fig. 8(c). This function consists of a number of well-separated δ-function peaks.

two points in question. If the correlations have inversion symmetry, $G_{\Gamma}^{(6)}(r)$ is real in this case. The precise procedure used in our numerical computations is described in Appendix B. The radially averaged *geodesic* correlation function $G_{\Gamma_0}^{(6)}(r)$ is plotted in Fig. 7 for $\kappa d=0.5$. The orientational correlation length can be found by fitting the envelope defined by the maxima of the curve to an exponential decay. The orientational correlation length is $\xi_6 \simeq 2.1d$, which is roughly the distance between the excess sevenfold disclinations predicted by Eq. (2.5). A breakup of orientational order on this scale is to be expected.[12]

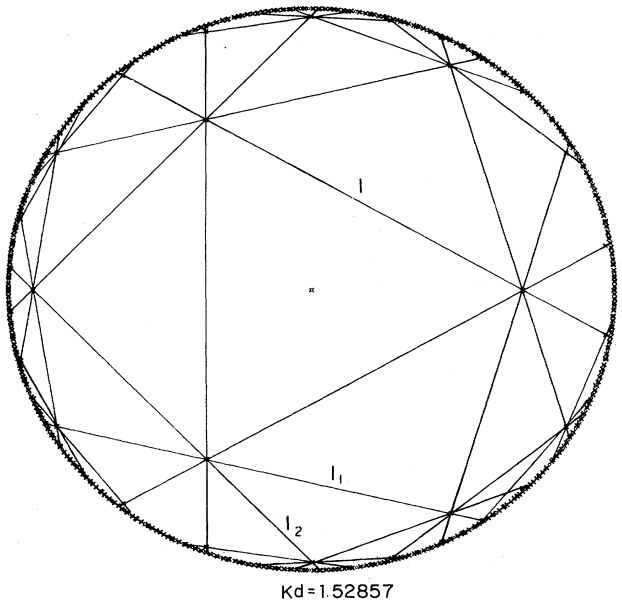

FIG. 10. Geodesic projection of the octagonal lattice ($\kappa d=1.528\,57$). A few geodesics, which appear as straight lines in the projection, are also shown.

Results for $g(r)$ and $G_{\Gamma_0}^{6}(r)$ for a variety of incommensurate curvatures are summarized in Table I.

D. Commensurate curvatures

A sequence of Bennett packings leading to a commensurate sevenfold lattice when $\kappa d=\kappa_7 d \approx 1.090\,55$ is shown in Fig. 8. An interesting commensurate-incommensurate transition takes place as every particle becomes seven-coordinated in the limit $\kappa \to \kappa_7$. As shown in Fig. 9, the radial distribution function for $\kappa=\kappa_7$ has δ-function Bragg peaks.

A commensurate eightfold lattice obtained for $\kappa d=\kappa_8 d=1.528\,57$ is shown in Fig. 10 using the geodesic projection discussed earlier. An infinite number of points fall on the extensions of every geodesic bond in this curved-space lattice. These are the analogs of Bragg planes in $H2$. Points at infinity are mapped onto the rim of the projection. Note that the intersecting Bragg "planes" l_1 and l_2 are *both* parallel to the Bragg plane l.

ACKNOWLEDGMENTS

It is a pleasure to acknowledge discussions with C. Henley, S. John, B. Shraiman, F. Spaepen, and A. Weinrib. This work was supported by the National Science Foundation, through the Materials Research Laboratory, and through Grant No. DMR-82-07431. One of us (D.R.N.) was supported by a grant from the Alfred P. Sloan Foundation.

APPENDIX A: GEODESIC DISTANCES IN $H2$

The formula (2.1) for the distance between two points in $H2$ along the geodesic line joining them is just the formula for great-circle distances on a sphere, analytically continued to imaginary sphere radii. We show here how (2.1) follows by explicit integration of the hyperbolic metric (1.1).

Consider two points A and B with corresponding polar coordinates (r_A,ϕ_A) and (r_B,ϕ_B) on a manifold of constant negative Gaussian curvature $K=-\kappa^2$. The equation of a geodesic in this space is[9]

$$\tanh(\kappa r)\cos(\phi-\phi_0)=\kappa k_0 , \tag{A1}$$

where k_0 and ϕ_0 are constants determined by the coordinates of A and B. It follows that, along a geodesic,

$$\frac{dr}{d\phi}=\frac{\sinh(\kappa r)\cosh(\kappa r)}{\kappa}\tan(\phi-\phi_0) , \tag{A2}$$

independent of k_0. The length of a geodesic joining points A and B can be calculated by integrating the metric (1.1):

$$\begin{aligned} d_{AB}&=\int_A^B ds=\int_A^B \{d^2r+[\sinh(\kappa r)/\kappa]^2 d^2\phi\}^{1/2} \\ &=\int_{\phi_A}^{\phi_B}\frac{\sinh(\kappa r)}{\kappa}d\phi[\cosh^2(\kappa r)\tan^2(\phi-\phi_0)+1]^{1/2} \\ &=k_0[1-(\kappa k_0)^2]^{1/2}\int_A^B \frac{d\phi}{\cos^2(\phi-\phi_0)-(\kappa k_0)^2} , \end{aligned} \tag{A3}$$

where we have used (A1) and (A2).

Performing the integration, we find

$$\kappa d_{AB}=\sinh^{-1}\left[\frac{\kappa k_0\sin(\phi_B-\phi_0)}{[\cos^2(\phi_B-\phi_0)-(\kappa k_0)^2]^{1/2}}\right]-\sinh^{-1}\left[\frac{\kappa k_0\sin(\phi_A-\phi_0)}{[\cos^2(\phi_A-\phi_0)-(\kappa k_0)^2]^{1/2}}\right]. \tag{A4}$$

Taking the cosh of both sides of this expression and using Eq. (A1) to eliminate κk_0, we find finally

$$\begin{aligned}\cosh(\kappa d_{AB})&=\cosh(\kappa r_A)\cosh(\kappa r_B)[1-(\kappa k_0)^2]-\sinh(\kappa r_A)\sinh(\kappa r_B)\sin(\phi_A-\phi_0)\sin(\phi_B-\phi_0)\\&=\cosh(\kappa r_A)\cosh(\kappa r_B)-\sinh(\kappa r_A)\sinh(\kappa r_B)\cos(\phi_A-\phi_B)\ .\end{aligned} \tag{A5}$$

APPENDIX B: ORIENTATIONAL CORRELATION FUNCTION

For an arbitrary configuration of atoms on a hyperbolic surface one can identify near neighbors via the Dirichlet construction. It is convenient to associate an orientational order parameter with every *particle,* rather than every bond. This is done by averaging Eq. (2.15) over all bonds terminating in a given particle. We are led to consider any two atoms A and B with N_A and N_B nearest neighbors located at $A_1,A_2,\ldots,A_{N_A}$ and $B_1,B_2,\ldots,B_{N_B}$, respectively.

A near-neighbor "bond" is defined to be the geodesic linking an atom wtih its near neighbor. There is also a unique geodesic, connecting atoms A and B. Below we calculate angles between this geodesic and nearest-neighbor bonds. If we know these angles $\theta_{A_1},\theta_{A_2},\ldots,\theta_{A_{N_A}}$, $\theta_{B_1},\theta_{B_2},\ldots,\theta_{B_{N_B}}$ then the radially averaged orientational-order correlation function for p-fold orientational symmetry is

$$G^p_{\Gamma_0}=\left\langle\left[\frac{1}{N_A}\sum_{n=1}^{N_A}\exp(ip\theta_{A_n})\right]\times\left[\frac{1}{N_B}\sum_{n=1}^{N_B}\exp(-ip\theta_{B_n})\right]\right\rangle, \tag{B1}$$

where we average overall pairs of points A and B in a configuration with a given length of a geodesic connecting them. We use the fact that angles do not change when parallel transported along a geodesic.[31] The equation for a geodesic on a uniform hyperbolic surface is given by Eq. (A1).

As discussed in Appendix A, the distance between B and an *arbitrary* point a along the geodesic BA is

$$\kappa d_{Ba}=\sinh^{-1}\left[\frac{\kappa k_0\sin(\phi_B-\phi_0)}{[\cos^2(\phi_B-\phi_0)-(\kappa k_0)^2]^{1/2}}\right]-\sinh^{-1}\left[\frac{\kappa k_0\sin(\phi_a-\phi_0)}{[\cos^2(\phi_a-\phi_0)-(\kappa k_0)^2]^{1/2}}\right]. \tag{B2}$$

The geodesic BA must be parametrized as in Eq. (A1). The unit tangent vector along the geodesic AB at point B is[32]

$$\vec{t}_B=\left[\frac{dr_B}{d(d_{BA})}\right]_{a=B}\vec{e}_r+\left[\frac{d\phi_B}{d(d_{BA})}\right]_{a=B}\vec{e}_\phi\ , \tag{B3}$$

where $\vec{e}_r$ and $\vec{e}_\phi$ are unit basis vectors for polar coordinates in $H2$. Using (B2) we find

$$c_r(B)\equiv\left[\frac{dr_B}{d(d_{Ba})}\right]\Bigg|_{a=B}=\frac{\kappa k_0}{[1-(\kappa k_0)^2]^{1/2}}\coth(\kappa r_B)\tan(\phi_B-\phi_0) \tag{B4a}$$

and

$$c_\phi(B)\equiv\left[\frac{d\phi_B}{d(d_{Ba})}\right]_{a=B}=\frac{\kappa^2 k_0}{[1-(\kappa k_0)^2]^{1/2}}\frac{1}{\sinh^2(\kappa r_B)}\ . \tag{B4b}$$

Note that both ϕ_0 and k_0 in (B2) depend on ϕ_B and r_B via Eq. (A1). Similarly, for the geodesic connecting point B to its near neighbor B_n, the unit tangent vector $\vec{t}_n$ has components

$$c_r(B_n)\equiv\left[\frac{dr_B}{d(d_{Bb})_n}\right]_{b_n=B}=\frac{\kappa k_n}{[1-(\kappa k_n)^2]^{1/2}}\coth(\kappa r_B)\tan(\phi_B-\phi_n)\ , \tag{B5a}$$

$$c_\phi(B_n)\equiv\left[\frac{d\phi_B}{d(d_{Bb})_n}\right]_{b_n=B}=-\frac{\kappa^2 k_n}{[1-(\kappa k_n)^2]^{1/2}}\frac{1}{\sinh^2(\kappa r_B)}\ , \tag{B5b}$$

where b_n is a point along the geodesic joining B to B_n, parametrized by the constants k_n and ϕ_n. If θ_{B_n} is the angle between $\vec{t}_B$ and $\vec{t}_n$, then

$$\cos(\theta_{B_n})=c_r(B)c_r(B_n)+\frac{\sinh^2(\kappa r_B)}{\kappa^2}c_\phi(B)c_\phi(B_n)\ . \tag{B6}$$

Substituting Eqs. (B4) and (B5) and using Eq. (B2) we find finally

$$\cos(\theta_B^n)=-\frac{\cosh^2(\kappa r_B)\tan(\phi_B-\phi_0)\tan(\phi_B-\phi_n)+1}{[\cosh^2(\kappa r_B)\tan^2(\phi_B-\phi_0)+1]^{1/2}[\cosh^2(\kappa r_B)\tan^2(\phi_B-\phi_n)+1]^{1/2}}\ . \tag{B7}$$

*Present address: Bell Telephone Laboratories, Murray Hill, NJ 07974.

[1]J. D. Bernal, Proc. R. Soc. London Ser. A 280, 299 (1964).

[2]J. L. Finney, Proc. R. Soc. London Ser. A 319, 479 (1970); 319, 495 (1970).

[3]C. H. Bennett, J. Appl. 43, 2727 (1972).

[4]P. Chaudhari and D. Turnbull, Science 199, 11 (1978).

[5]F. C. Frank, Proc. R. Soc. London Ser. A 215, 43 (1952).

[6]P. Steinhardt, D. R. Nelson, and M. Ronchetti, Phys. Rev. Lett. 47, 1297 (1981); Phys. Rev. B 28, 784 (1983).

[7]H. S. M. Coxeter, Ill. J. Math. 2, 746 (1958).

[8]H. S. M. Coxeter, *Regular Polytopes* (Dover, New York, 1973).

[9]H. S. M. Coxeter, *Introduction to Geometry* (Wiley, New York, 1969).

[10]M. Kléman and J. F. Sadoc, J. Phys. (Paris) Lett. 40, L569 (1979).

[11]N. D. Mermin, Rev. Mod. Phys. 51, 591 (1979).

[12]D. R. Nelson, Phys. Rev. Lett. 50, 982 (1983); Phys. Rev. B 28, 5515 (1983).

[13]F. C. Frank and J. S. Kasper, Acta Crystallogr. 11, 184 (1958); 12, 483 (1959).

[14]R. Collins, in *Phase Transitions and Critical Phenomena,* edited by C. Domb and M. S. Green (Academic, New York, 1976), Vol. 2.

[15]J. P. McTague, D. Frenkel, and M. Allen, in *Ordering in Two Dimensions,* edited by S. Sinha (North-Holland, Amsterdam, 1980).

[16]A. S. Nowick and S. Mader, IBM J. Res. Dev. Sept.-Nov., 358 (1965).

[17]D. R. Nelson, M. Rubinstein, and F. Spaepen, Philos. Mag. A 46, 105 (1982).

[18]M. Rubinstein and D. R. Nelson, Phys. Rev. B 26, 6254 (1982).

[19]D. R. Nelson, Phys. Rev. B 27, 2902 (1983).

[20]D. R. Nelson, in *Topological Disorder in Condensed Matter,* edited by F. Yonezawa and T. Ninomiya (Springer, Berlin, 1983).

[21]T. Fujiwara, in *Topological Disorder in Condensed Matter,* Ref. 20.

[22]Particles packed on a sphere have been studied previously by W. Schreiner and K. W. Kratky, J. Chem. Soc. Faraday Trans. 2 78, 379 (1982).

[23]M. R. Hoare, Ann. N.Y. Acad. Sci. 279, 186 (1976).

[24]J. P. Gaspard, R. Mosseri, and J. F. Sadoc, Proceedings of the Conference on Structure of Non-Crystalline Materials, Cambridge, England, 1982 (in press).

[25]D. S. Boudreaux and J. M. Gregor, J. Appl. Phys. 48, 152 (1977); 48, 5057 (1977).

[26]For an elementary introduction to differential geometry in $H2$, see Chapters 19—21 of Ref. 9.

[27]D. Hilbert and S. Cohn-Vossen, *Geometry and the Imagination* (Chelsea, New York, 1952), Chap. IV.

[28]J. F. Sadoc, J. Dixmier, and A. Guinier, J. Non-Cryst. Solids 12, 46 (1973).

[29]C. S. Cargill, Ann. N.Y. Acad. Sci. 279, 208 (1976).

[30]E. Fradkin, B. A. Huberman, and S. H. Shenker, Phys. Rev. B 18, 4789 (1978).

[31]See, e.g., L. D. Landau and I. M. Lifshitz, *The Classical Theory of Fields* (Pergamon, New York, 1971), Chap. 11.

[32]See, e.g., C. W. Misner, K. S. Thorne, and J. A. Wheeler, *Gravitation* (Freeman, San Francisco, 1971).